DFT and experimental study of nano red phosphorus anchoring on sulfurized polyacrylonitrile for lithium-ion battery

Yang Wang [a], Pengjian Zuo *[a], Shaobo Ma [a], Bingxing Xie [a], Zhenjiang Yu [a] and Geping Yin [a]

[a] Institute of Advanced Chemical Power Source, School of Chemical Engineering and Technology, Harbin Institute of Technology, Harbin, 150001, China

*Corresponding author. E-mail: zuopj@hit.edu.cn (Pengjian. Zuo);

Preparation of nano red phosphorus

The preparation of nano red phosphorus was implemented through a solvothermal process of ethylenediamine as our previous work. [1] While the reaction condition was setted as 120 °C at 120 for 12 h. After cooling down to room temperature, the bottom precipitation was washed with deionized water and alcohol for three times, ultrasonic treatment for 2h under 400W condition. After vacuum drying for 12 h at 60 °C, the brown-yellow nano RP was obtained.

Preparation of the SPAN

1.0 g of monomer acrylonitrile (AN, Aldrich), 0.5 g of sublimed sulfur (Aladdin) and were dispersed in 10 ml ethanol medium, followed by a balling-milling process for 8 h. After centrifuged and washed with ethanol for several times, the mixture was dried at 70 ℃ in a vacuum oven for 12 h. Then the mixture was sealed in a quartz tube filled with argon gas and heated at 400 ℃ for 2 h. After cooling down, the obtained product denoted as SPAN was disposed with grinding and sieving (200 mesh).

Preparation of the SPAN-RP

The obtained SPAN were sealed in jar mills under an Ar atmosphere condition, and they were ball milled for 8h at a 400 rpm speed. Taking a certain quality of SPAN and nano RP, mixed them at a ratio of 3:7 in ethanol medium, followed by an ultrasonic treatment for 2h under 400W condition. Then the mixture was dried at 70 ℃ in a vacuum oven for 12 h. After cooling down, the obtained mixture denoted as SPAN-RP.

Cell Preparation and Electrochemical Characterization

The working electrode was fabricated by mixing the active material (RP or SPAN-RP, 70 wt%) with Super P (20 wt%) and polyvinylidene fluoride (10 wt%) in N-methyl-2-pyrrolidone. The resulting homogeneous slurry was casted onto copper foil substrates, dried at 120℃ for 12 h in a vacuum oven. The mass loading of active material is 0.4~0.5 mg cm^{-2}. Electrochemical measurements were performed in CR2025-type coin cells consisting of metallic lithium as the counter electrode and

Celgard 2400 was used as separator. The electrolyte was comprised of 1 M $LiPF_6$ in a mixed solution of ethylene carbonate (EC) and diethyl carbonate (DEC) with 1:1 volume fraction. For the potassium ion battery, the K metal was used as the counter/reference electrode and Whatman GF/F microfiber glass membranes were used as separators. The electrolyte was 0.75 M KPF_6 in a mixture of ethylene carbonate (EC) and diethyl carbonate (DEC) with a volume ratio of 1:1. Galvanostatic cycling tests of the assembled cells were carried out on a Neware battery test system at a voltage range between 0.01 and 2.0 V.

Computational Methods

All density functional theory calculations were performed using the Guassian09 program package.[2] No geometric constraints were assumed in geometry optimization. The nonlocal correlation functional of Lee, Yang, and Parr [3] (B3LYP) with the 6-31++G** basis set was used for H, C, S, N and P atoms.[4] All reported charges are Mulliken local charges (a.u.). The relative energies of the reactants, products, intermediates presented in this study were zero-point-energy (ZPE) obtained from frequency calculations at the same level of optimization. All stationary points were characterized as the minima (no imaginary frequency) via Hessian calculation.

An important reference point for this calculation is the adsorption energy $E_{(ads)}$ for P_4 molecule adsorbed on isolated PAN and SPAN molecule. In this paper, we used the following definitions for adsorption energy.

$E_{(ads)} = E_{(PAN\text{-}RP)} - E_{(PAN)} - E_{(RP)}$; $E_{(ads)} = E_{(SPAN\text{-}RP)} - E_{(SPAN)} - E_{(RP)}$

$E_{(PAN\text{-}RP)}$ and $E_{(SPAN\text{-}RP)}$ is the total energy of adsorption system: PAN-RP and

SPAN-RP; $E_{(PAN)}$, $E_{(SPAN)}$ and $E_{(RP)}$ denote the energy of the PAN, SPAN and P_4 molecule respectively.

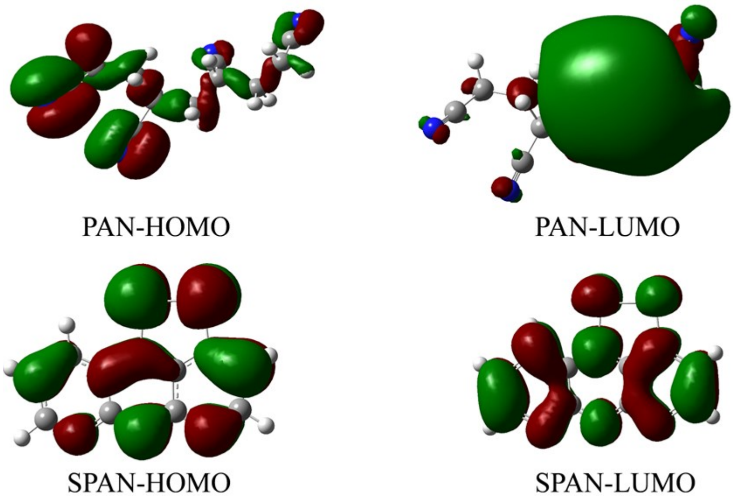

Figure S1. The HOMO and LUMO orbital distribution of PAN and SPAN.

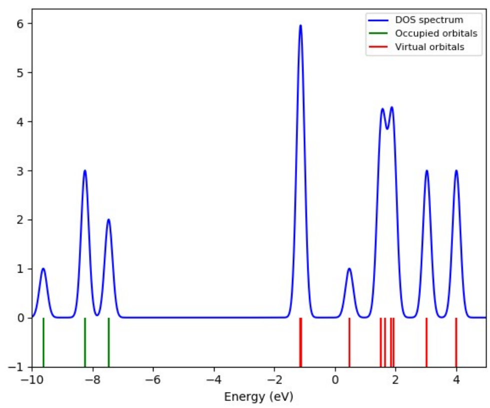

Figure S2. The density of states (DOS) and bandgap of molecular orbitals (MOs) for P_4 molecular.

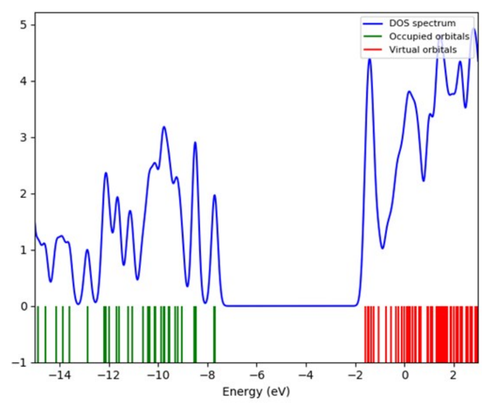

Figure S3. The density of states (DOS) and bandgap of molecular orbitals (MOs) for PAN-P_4 molecular.

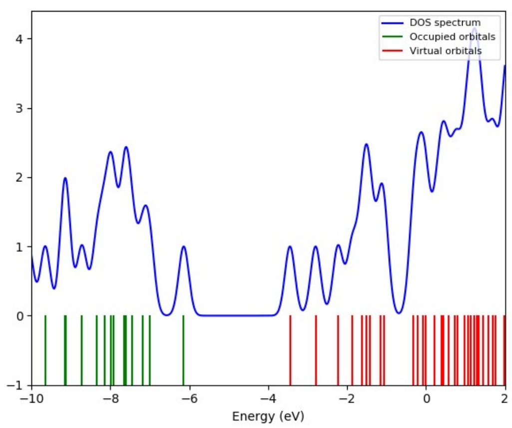

Figure S4. The density of states (DOS) and bandgap of molecular orbitals (MOs) for SPAN-P_4 molecular.

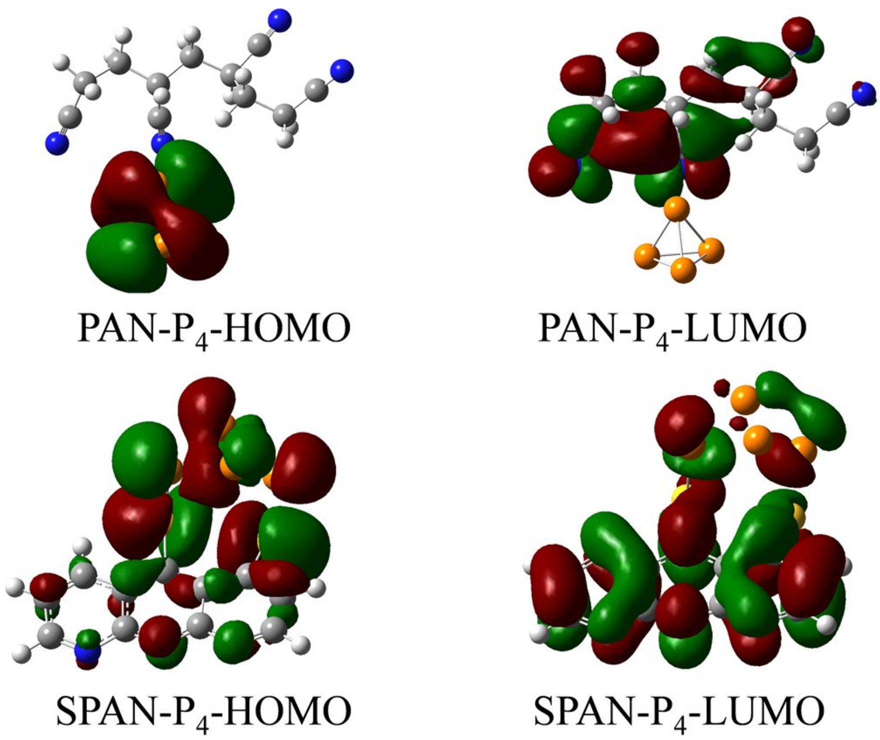

Figure S5. The HOMO and LUMO orbital distribution of PAN-P_4 and SPAN-P_4.

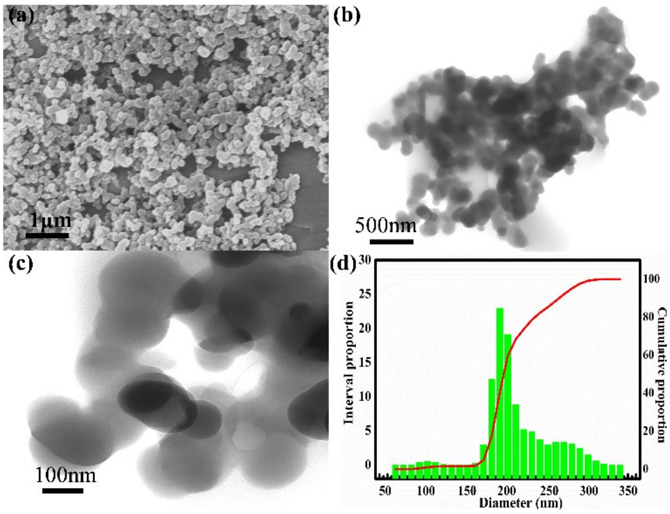

Figure S6. (a) The SEM image of the RP nanoparticles. (b-c) The TEM images of the RP nanoparticles. (d) The curve of particle size distribution of the RP nanoparticles.

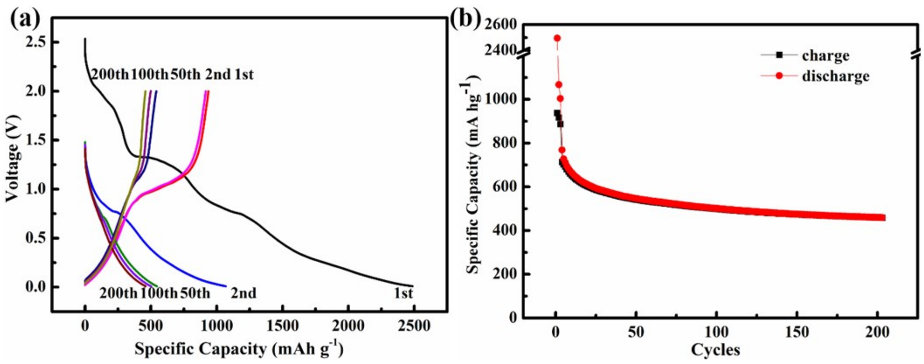

Figure S7. The voltage profiles and the cycling performance of nano RP at 0.5C current density.

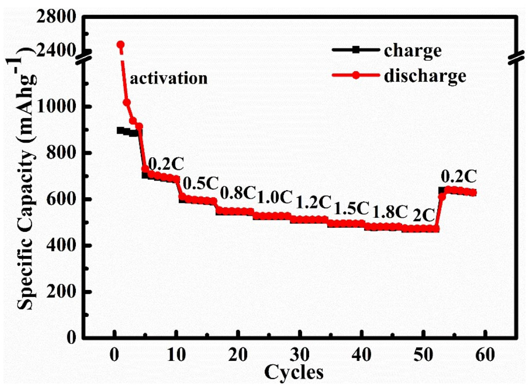

Figure S8. The rate performance of nano RP anode for LIBs.

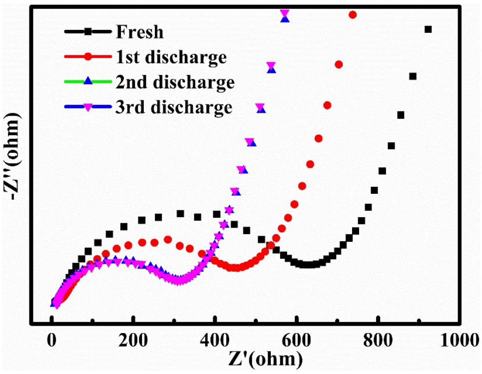

Figure S9. The EIS of RP anodes measured at the fresh state and three different fully discharged states for LIBs.

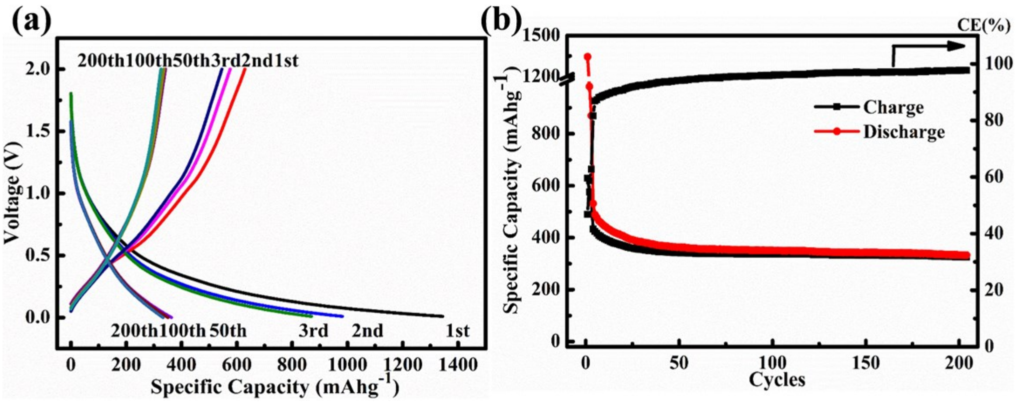

Figure S10. (a) The voltage profiles and (b) the cycling performance of nano RP anode at a current density of 0.2C for potassium ion battery.

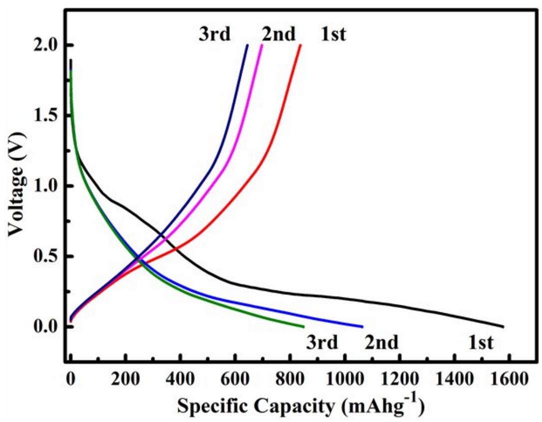

Figure S11. The voltage profiles of nano RP anode at a current density of 50 mA g^{-1} for potassium ion battery.

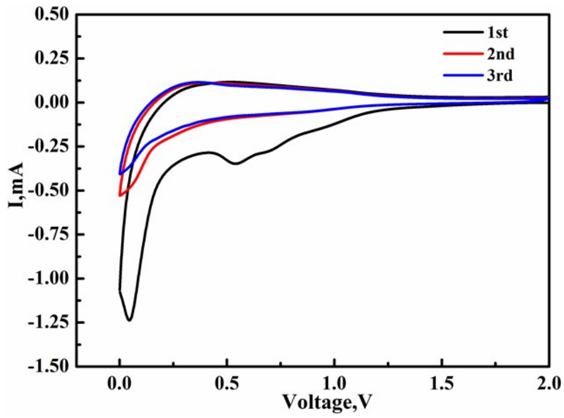

Figure S12. The cyclic voltammograms of nano RP at a scan rate of 0.2 mV s^{-1} for potassium ion battery.

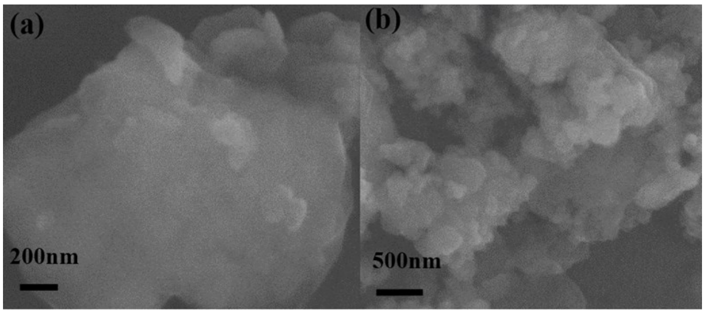

Figure S13. The SEM images of (a) SPAN and (b) the SPAN-RP composite material.

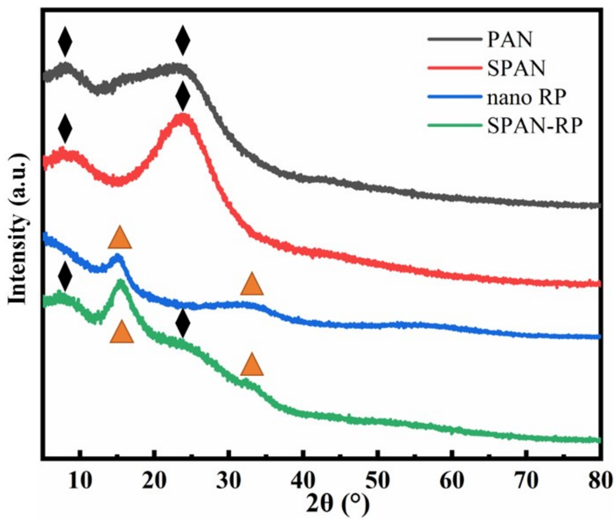

Figure S14. The XRD patterns of PAN, SPAN, nano RP and SPAN-RP four samples.

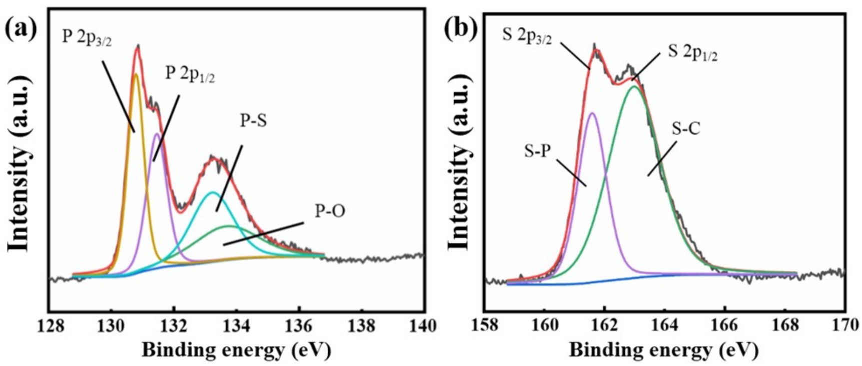

Figure S15.The high-resolution XPS spectrum of P 2p and S 2p of SPAN-RP.

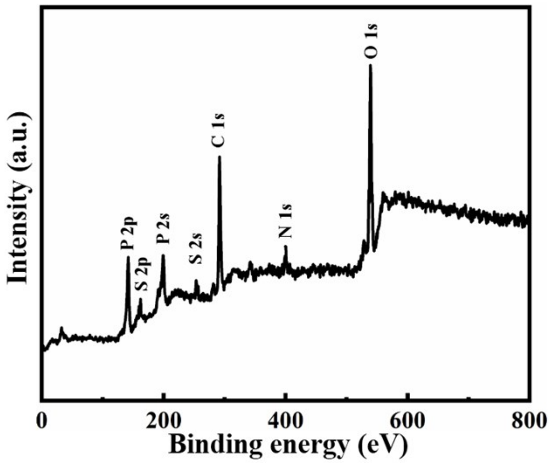

Figure S16.The XPS spectra survey scan of P, S, C, N and O elements in SPAN-RP.

The high-resolution and survey spectra of X-ray photoelectron spectroscopies (XPS) of SPAN-RP are shown in Figure S15, 16. In Figure S15, 16, high-resolution and survey spectra of X-ray photoelectron spectroscopies (XPS) were obtained for SPAN-RP. Two peaks at ~130.5 and ~131.5 eV (Figure S15a) correspond to the 2p3/2 and 2p1/2 states of phosphorus, respectively. The peaks at ~134 and ~133 eV (Figure S15a) correspond to the P-O bond and P-S bond, respectively. [5, 6] The S 2p XPS spectrum further confirms the P-S bond in SPAN-RP (Figure S15b), and the two intense peaks at ~161 and ~163 eV are assigned to S-P and S-C bonds, respectively. [5-8]

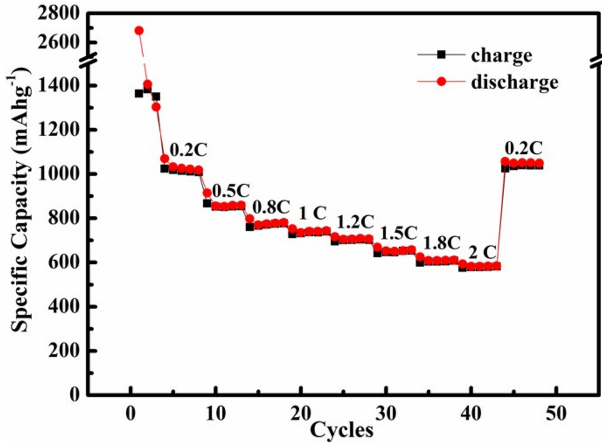

Figure S17. The rate performance of SPAN-RP anode for LIBs.

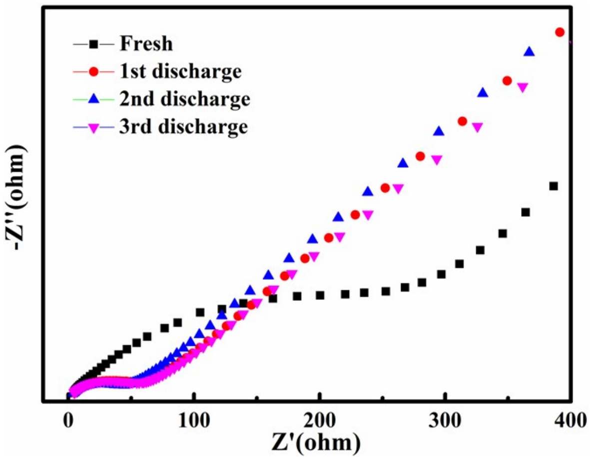

Figure S18. The EIS of SPAN-RP anode measured at the fresh state and three different fully discharged states for LIBs.

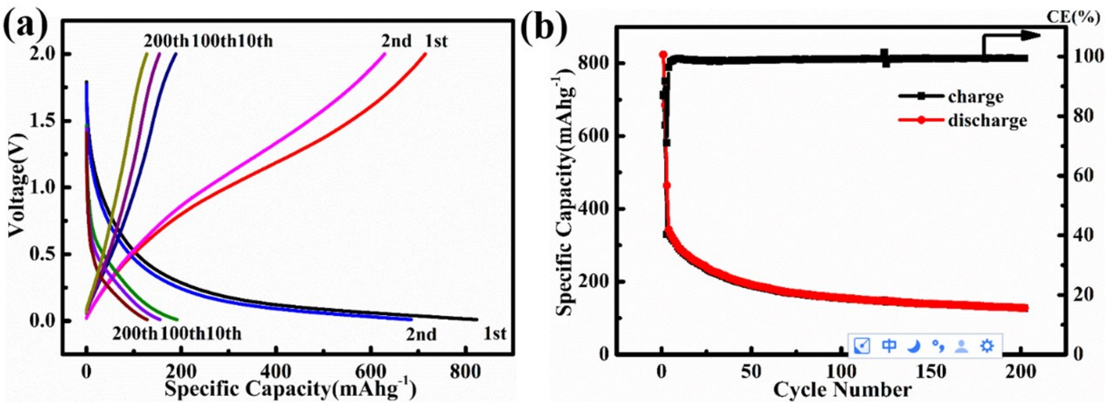

Figure S19. The voltage profiles (a) and the cycling performance and columbic efficiency (b) of SPAN anodes for LIBs at a current density of 0.1 A g^{-1}.

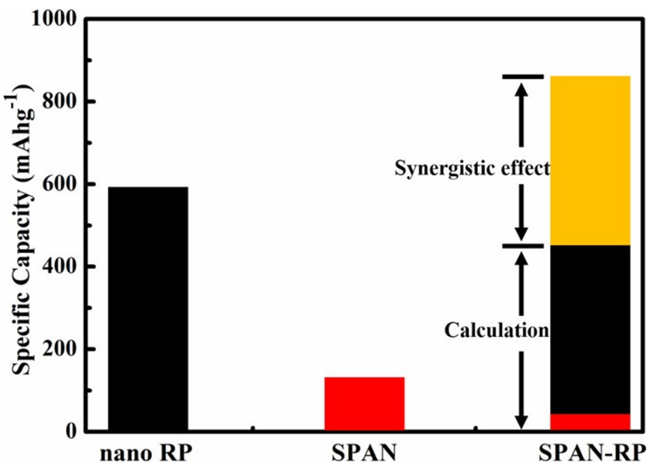

Figure S20. The specific capacity of nano RP, SPAN, and SPAN-RP after 200 cycles. The yellow rectangle indicates the increased capacity due to the synergistic effect between SPAN and nano RP.

The specific capacity contributions of nano RP, SPAN, and SPAN-RP after 200 cycles are shown in Figure S20. In Figure S20, after 200 cycles, the nano RP and SPAN-RP keep specific capacities of 590 mAh g^{-1} and 860 mAh g^{-1} at 0.2C, respectively. The pristine SPAN keeps a specific capacity of 130 mAh g^{-1} after 200 cycles at a current density of 0.1 A g^{-1} (Figure S19). According to the mass ratio (7:3) of RP/SPAN, the calculated total capacity of SPAN-RP based on the above practical discharge capacity of RP and SPAN after 200 cycles is 452 mAh g^{-1} ($590 \times 70\% + 130 \times 30\% = 452$ mAh g^{-1}). However, the practical discharge capacity of SPAN-RP can be up to 860 mAh g^{-1} (Figure 4d and Figure S20), indicating the synergistic effect between SPAN and nano RP on improving the electrochemical performance.

Table S1. The energy of HOMO, LUMO, and HOMO-LUMO gap of different molecular.

(B3LYP/6-31g++(d, p) basis set; isovalue = 0.02; eV)

	HOMO	LUMO	HOMO-LUMO gap
PAN	-9.09	-1.31	7.77
SPAN	-6.19	-2.94	3.24
P4	-7.46	-1.14	6.32
PAN-P4	-7.68	-1.57	6.11
SPAN-P4	-6.14	-3.44	2.69

The Cartesian coordinates of the species in DFT calculation

PAN

Atomic	Coordinates (Angstroms)		
Number	X	Y	Z
C	-2.92064100	-1.55447900	-0.11726500
C	-1.65701600	-0.75531600	-0.52046700
H	-2.85891600	-2.56246100	-0.54236500
H	-2.97083400	-1.67965000	0.97088900
C	-1.24423000	0.36027300	0.46898100
H	-0.82861400	-1.46781100	-0.56892300
H	-1.78890100	-0.33646600	-1.52377700
C	0.01506300	1.14394800	0.01392700
H	-1.02623600	-0.11016000	1.43751400
H	-0.20541200	1.66169900	-0.92611900
H	0.22903600	1.91442800	0.76196100
C	-4.18086600	-0.96991300	-0.58854300
C	-2.31962300	1.33538100	0.71240400
N	-5.17831900	-0.54395900	-1.00258500
N	-3.13186800	2.13905700	0.91918600
C	1.29564400	0.29328700	-0.20249700

C	2.50202600	1.22136000	-0.49699200
H	1.14696700	-0.36257900	-1.07041900
C	1.52115400	-0.58054000	0.96059800
C	3.69919100	0.55629200	-1.20744500
H	2.14496700	2.01656000	-1.16019600
H	2.83278400	1.70116800	0.42931500
N	1.61648700	-1.25809600	1.89910500
H	3.36577700	0.06096100	-2.12781600
C	4.44622600	-0.42042300	-0.40741200
N	5.06694200	-1.18732200	0.20439100
H	4.40512700	1.33733900	-1.51247500

SPAN

Atomic Number	Coordinates (Angstroms) X	Y	Z
C	2.56996300	2.39905800	0.00005800
C	0.38068400	1.68948700	-0.00003300
C	0.83538300	0.32489600	-0.00000700
C	2.22552100	0.03666400	-0.00000200
C	3.12025500	1.08394500	0.00001600
C	-0.08808700	-0.71958200	-0.00000300
C	-1.46319000	-0.41519300	0.00000100
C	-1.81601200	0.99361200	0.00002300
C	-4.06127400	0.44882400	0.00000400
C	-3.80941800	-0.95414800	-0.00000200
C	-2.50677600	-1.37931300	-0.00000100
H	3.26379800	3.23890000	0.00002700
H	4.19480900	0.94215800	0.00000800
H	-5.09173400	0.80266400	-0.00000600
H	-4.63710700	-1.65536000	-0.00000900
H	-2.26644800	-2.43941400	-0.00000700
N	1.29135600	2.71284800	0.00001700
N	-0.92026700	1.99387600	0.00000000
N	-3.13361000	1.37699900	0.00001000
S	0.59685200	-2.34778800	-0.00000400
S	2.62515000	-1.68499400	-0.00002900

PAN-RP

Atomic Number	Coordinates (Angstroms) X	Y	Z
C	-2.82278600	-2.21555700	0.15549400

C	-2.36630600	-0.84439300	-0.39952900
H	-2.08171800	-2.97570900	-0.11557200
H	-2.86142500	-2.19748300	1.25116900
C	-2.87555900	0.38438000	0.39003300
H	-1.27371000	-0.82985900	-0.35454200
H	-2.65183700	-0.75710500	-1.45323800
C	-2.38253400	1.73303500	-0.19788200
H	-2.50571500	0.30218100	1.42124700
H	-2.77656900	1.84704900	-1.21385200
H	-2.80510200	2.54539600	0.40256800
C	-4.11625200	-2.67874200	-0.35870200
C	-4.34386500	0.44042400	0.47752700
N	-5.11307300	-3.07965400	-0.79853700
N	-5.49852000	0.53745600	0.55372300
C	-0.84221100	1.91326800	-0.26356300
C	-0.49805200	3.34531600	-0.74403400
H	-0.42686000	1.20069400	-0.98823100
C	-0.24097200	1.58737900	1.03993400
C	0.94289300	3.55104700	-1.25731800
H	-1.16718400	3.57142400	-1.58108300
H	-0.72160100	4.06590200	0.04879400
N	0.16810900	1.28358900	2.08372900
H	1.19385400	2.78726400	-2.00356300
C	1.98600600	3.54507700	-0.22578100
N	2.83139800	3.56620300	0.56961000
H	0.99885200	4.51849400	-1.76948300
P	2.16080000	-0.94866100	-0.95877000
P	3.76346500	-0.68036900	0.54394500
P	2.13853200	-2.13570200	0.91821600
P	3.65196600	-2.55518900	-0.65012200

SPAN-RP

Atomic Number	Coordinates (Angstroms) X	Y	Z
C	0.36190300	3.76302200	0.51773300
C	1.72839200	1.91960900	0.35097600
C	0.66896300	1.09773600	-0.23563900
C	-0.57703800	1.77897800	-0.51664400
C	-0.70926000	3.09588300	-0.13533500
C	0.99167400	-0.25898300	-0.48071400
C	2.31493100	-0.71309700	-0.26294400
C	3.29027700	0.22728300	0.23690100
C	4.95971200	-1.35623600	0.19068900

C	4.07117500	-2.37094100	-0.27608000
C	2.75917200	-2.05086700	-0.49632000
H	0.22938500	4.79499300	0.84014100
H	-1.62451700	3.63444600	-0.35325300
H	6.00811500	-1.59969500	0.35936000
H	4.44154500	-3.37635600	-0.44825200
H	2.05268100	-2.79135100	-0.85196100
N	1.53009100	3.22208900	0.73885500
N	2.97237900	1.48229700	0.55715700
N	4.60218700	-0.12212400	0.44483400
S	-0.21186500	-1.44790100	-1.07363200
S	-1.91722200	1.16434600	-1.55026200
P	-3.45057300	0.36279000	-0.21390200
P	-3.43460400	-1.86751400	0.24680700
P	-1.24852000	-2.02958800	0.75037600
P	-2.52855700	-0.39870800	1.67636000

References:

(1) Y. Wang, M. He, S. Ma, C. Yang, M. Yu, G. Yin and P. Zuo. Low-Temperature Solution Synthesis of Black Phosphorus from Red Phosphorus: Crystallization Mechanism and Lithium Ion Battery Applications. *J Phys Chem Lett*, **2020**, 11, 2708-2716.

(2) Frisch, M.; Trucks, G.; Schlegel, H.; Scuseria, G.; Robb, M.; Cheeseman, J.; Scalmani, G.; Barone, V.; Mennucci, B., Petersson., GA et al. Gaussian09, Rev. C. 01; Gaussian. Inc.: Wallingford, CT **2010**.

(3) Lee, C.; Yang, W.; Parr, R. G. Development of the Colle-Salvetti Correlation-Energy Formula into a Functional of the Electron Density. *Phys. Rev. B* **1988**, *37*, 785.

(4) Andersson, M. P.; Uvdal, P. New Scale Factors for Harmonic Vibrational Frequencies Using the B3LYP Density Functional Method with the Triple-ζ Basis Set 6-311+ G (d, p). *J. Phys. Chem. A* **2005**, *109*, 2937-2941.

(5) Xu, Z. L., Lin, S., Onofrio, N., Zhou, L., Shi, F., et al. Exceptional catalytic effects of black phosphorus quantum dots in shuttling-free lithium sulfur batteries. N*ature communications*, **2018**,

9 (1), 1-11.

(6) Hu, Y., Li, B., Jiao, X., Zhang, C., Dai, X., et al. Stable Cycling of Phosphorus Anode for Sodium-Ion Batteries through Chemical Bonding with Sulfurized Polyacrylonitrile. *Advanced Functional Materials*, **2018**, 28 (23), 1801010.

(7) Kong, W., Wen, Z., Zhou, Z., Wang, G., Yin, J., Cui, L., Sun, W. A self-healing high-performance phosphorus composite anode enabled by in situ preformed intermediate lithium sulfides. *Journal of Materials Chemistry A*, **2019**, 7 (47), 27048-27056.

(8) Yan, J., Li, W., Feng, P., Wang, R., Jiang, M., Han, J., et al. Enhanced Na^+ pseudocapacitance in a P, S co-doped carbon anode arising from the surface modification by sulfur and phosphorus with C–S–P coupling. *Journal of Materials Chemistry A*, **2020**, 8 (1), 422-432.